Supporting Information

Densely Accessible Fe/Co-N_x Dual-atom Sites Coupled Core-shell Co_3Fe_7@C as an Efficient Bifunctional Oxygen Electrocatalyst for Rechargeable Zinc-air Batteries

Katam Srinivas[a,1], Hesheng Yu[a,1], Zhuo Chen[b], Anran Chen[c], Ming-qiang Zhu[b,*], Yuanfu Chen[a,*]

[a] *School of Integrated Circuit Science and Engineering, and State Key Laboratory of Electronic Thin Films and Integrated Devices, University of Electronic Science and Technology of China, Chengdu 610054, Sichuan, China*

[b] *College of Mechanical and Electronic Engineering, Northwest A&F University, Yangling 712100, Shaanxi, China*

[c] *School of Materials and Energy, Yunnan University, Kunming 650091, Yunnan, China*

[1] These authors contributed equally to this work.

*Corresponding authors.

E-mail addresses: zmqsx@nwsuaf.edu.cn (M.-q. Zhu), yfchen@uestc.edu.cn (Y. Chen).

1. Experimental Section

Absolute ethanol and the distilled water were used in washing the materials throughout the investigations.

1.2 Structural characterizations

Scanning electron microscope (SEM) images were carried out on a ZEISS Gemini 300. Transmission electron microscopy (TEM), high resolution TEM (HETEM), high angle annular dark field scanning transmission electron microscopy (HAADF-STEM), and element mapping analysis images were examined on a Talos F200X G2 with superX spectroscopy equipment. Aberration-corrected HAADF-STEM (AC HAADF-STEM) images were carried out on FEI-Themis Z. Notably, Fe_3Co-NC@900 was washed with 1 M HNO_3 solution at 80 ^oC for 24 hours, followed by 1 M KOH wash at room temperature for 16 hours, in order to extensively eliminate the high magnetic Co_3Fe_7 alloy particles prior to AC-HAADF-STEM test. X-ray diffraction (XRD) data were tested on a Rigaku Smartlab. Raman spectra data were measured on a Renishaw confocal microscope. X-ray photoelectron spectroscopy (XPS) data were obtained on a Thermo Scientific K-Alpha. N_2 adsorption/desorption isotherms (NADI) were obtained on a Micromeritics ASAP 2460 at 77 K. Inductively coupled plasma optical emission spectroscopy (ICP-OES) results were gained on a PE Avio 200.

1.3 Electrochemical characterizations

Electrochemical **ORR** measurements were carried out in O_2- and N_2-saturated 0.1 M KOH by using an electrochemical workstation (Pine, WaveDriver20) equipped with three

electrodes. Wherein the catalyst-loaded rotating disc electrode (RDE, Pine, 5 mm; for CV, LSV, CSCA, CV cycling, *i-t*, and methanol poisoning) and a rotating-ring disc electrode (RRDE, Pine, N = 0.37; for electron transfer number and H_2O_2 yield) were used as working electrodes, while the Hg/HgO electrode and Pt wire were used as the reference and counter electrodes, respectively.

Working electrodes were prepared by sonicating 5 mg of catalyst powder in 1 mL of mixed solvents (V_{water} : $V_{ethanol}$ = 3: 1) for 5 minutes. To which, 50 μL of Nafion ink was injected and ultrasonicated for an additional 30 min. Afterwards, 15 μL of catalyst ink was loaded on RDE and RRDE. The loading amounts of all the catalysts, including 20 wt.% Pt/C for ORR, were 0.29 mg cm^{-2}. All measured potentials were corrected versus the reversible hydrogen electrode (RHE) using the Nernst equation ($E_{RHE} = E_{(Hg/HgO)} + 0.0591 \times pH + 0.098$). The cyclic voltammetry (CV) curves were detected from 0.2 to 1.0 V on RDE (50 mV s^{-1}). The linear sweep voltammetry (LSV) curves were investigated from 0.2 to 1.1 V (10 mV s^{-1}, 400-2500 rpm). Cyclic step chronoamperometry (CSCA) was conducted to measure the solution resistance by adding an instantaneous 50 mV step potential at 8 ms. The final LSV data was obtained by subtracting the background current measured in N_2-saturated electrolyte and performing *iR* compensation using the CSCA results. The CV cycling tests were carried out from 0.6 to 1.0 V for continuous 2,000 cycles (200 mV s^{-1}). The long-term durability experiments were executed by a chronoamperometry test on RDE at 0.6 V for 4,500 s (at 1600 rpm). Methanol tolerance tests were carried out by adding 20 mL of methanol to 80 mL of 0.1 M KOH electrolyte.

The Koutecky–Levich equation was provided to evaluate the values of electron transfer number (*n*).

$$\frac{1}{j} = \frac{1}{j_d} + \frac{1}{j_k} = \frac{1}{B\omega^{1/2}} + \frac{1}{j_k}$$

$$B = 0.2nFC_0D^{2/3}V^{-1/6}$$

Wherein, *j*: measured current density; j_k: kinetic current density; j_d: diffusion-limited current density; ω: the angular velocity of the disk (rad s^{-1}); *F*: Faraday constant (96485 C mol^{-1}); C_0: bulk concentration of O_2 (1.2×10^{-6} mol cm^{-3}); D_0: diffusion coefficient of O_2 in 0.1 M KOH (1.9×10^{-5} cm^2 s^{-1}); *V*: kinematic viscosity of the electrolyte (0.01 cm^2 s^{-1}).

The H_2O_2 yield and '*n*' were further detected on RRDE. The LSV was obtained from 1.1 to 0.1 V (5 mV s^{-1}, 1600 rpm). And its ring potential was set at 1.3 V. Used the subsequent equations to calculate their specific values:

$$H_2O_2(\%) = 200 \times \frac{\frac{I_r}{N}}{I_d + \frac{I_r}{N}}$$

$$n = 4 \times \frac{I_d}{I_d + \frac{I_r}{N}}$$

Wherein, I_r: ring current; I_d: disk current; *N*: collection efficiency of the Pt ring (N = 0.37).

Similarly, the same catalyst ink was loaded (5 μL) on a glassy carbon working electrode (GCE; 3 mm diameter) to evaluate the **OER** performance tests on a CHI 660D

electrochemical workstation in 0.1 M KOH. The reference Ir/C catalyst ink was also prepared in the same manner and loaded on polished GCE (5 μL on 3 mm GCE; loading amount was 0.26 mg cm^{-2}). Herein, the three-electrode system is assembled by a catalyst-loaded GCE working electrode, a graphite counter electrode, and a Hg/HgO reference electrode. LSV curves were acquired by scanning the potential from 0 to 0.8 V versus the Hg/HgO electrode with a scanning speed of 5 mV s^{-1}. The electrochemical impedance spectroscopy (EIS) tests were performed from 0.1 to 100 kHz. CV cycling tests were carried out on GCE electrodes, while the chronoamperometric *i-t* tests were carried out on carbon cloth current collectors (loading amount = 2 mg cm^{-2}).

A rechargeable **Zn-Air battery** was constructed in a 6 M KOH aqueous electrolyte consisting of 0.2 M $Zn(Ac)_2$ using a CHI 660D electrochemical workstation. Polished zinc sheet was used as a metal anode (thickness of 0.3 mm), and the bifunctional electrocatalyst-loaded carbon paper was employed as air cathode. Electrocatalyst ink preparation is the same as above, and the obtained homogeneous link was loaded on carbon paper and dried in a 50 ^{o}C electric oven before assembling the Zn-air battery. While Pt/C+Ir/C mixed catalyst ink was also prepared in the same method by dispersing 5 mg of both catalysts (1:1 wt.%) in a mixed solution of 750 μL of water, 250 μL of deionized water, and 50 μL of Nafion ink by ultrasonication for 30 min. The homogenous ink was dropped onto the carbon paper, and the mass loading of the catalysts was 1.0 mg cm^{-2}. Electrolyte was replaced by pausing the experiment in order to check the rechargeability of a ZAB during the charge-discharge cycling test. All the electrochemical data of the as-prepared electrocatalysts presented in this article has been tested twice to make sure all the results are reliable and reproducible.

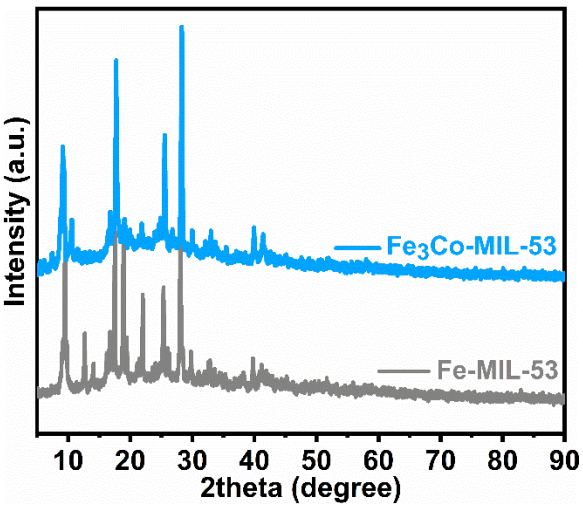

Fig. S1. Powder XRD patterns of Fe-MIL-53, and Co-doped Fe_3Co-MIL-53.

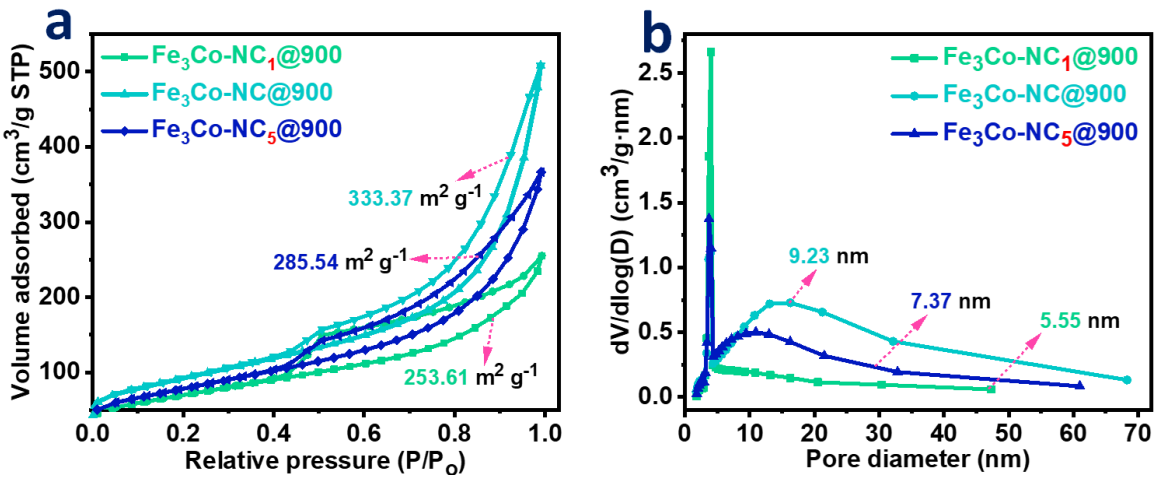

Fig. S2. (a) BET SSA profile of Fe_3Co-NC_1@900, Fe_3Co-NC@900 and Fe_3Co-NC_5@900, and (b) the corresponding BJH desorption curve.

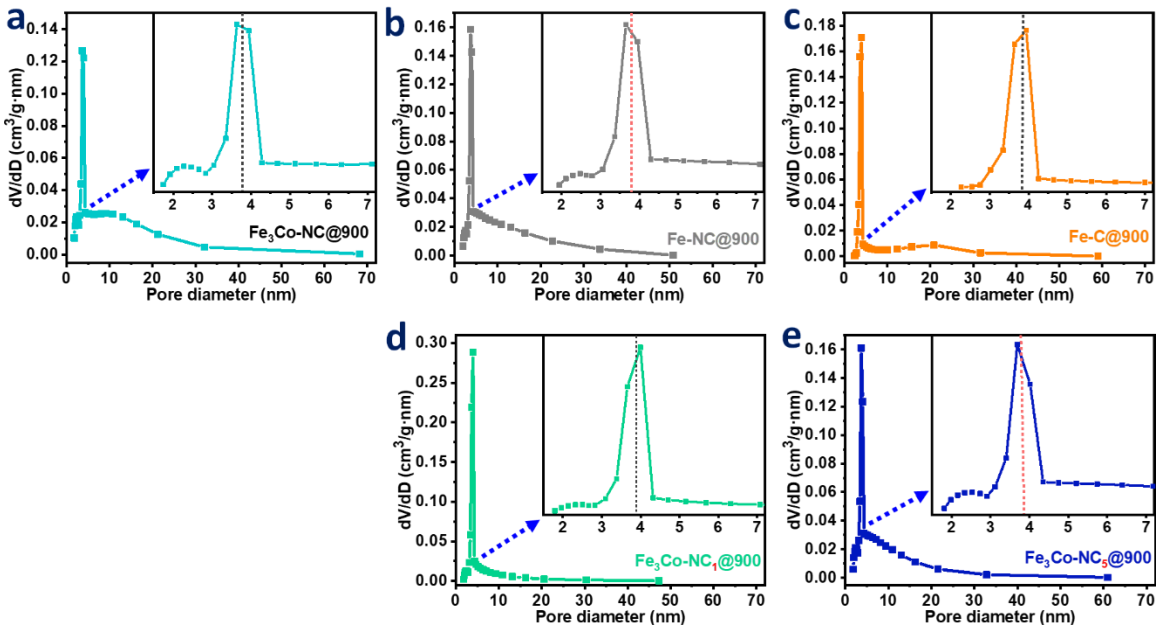

Fig. S3. (a-e) BJH desorption curves of MIL-derived electrocatalysts.

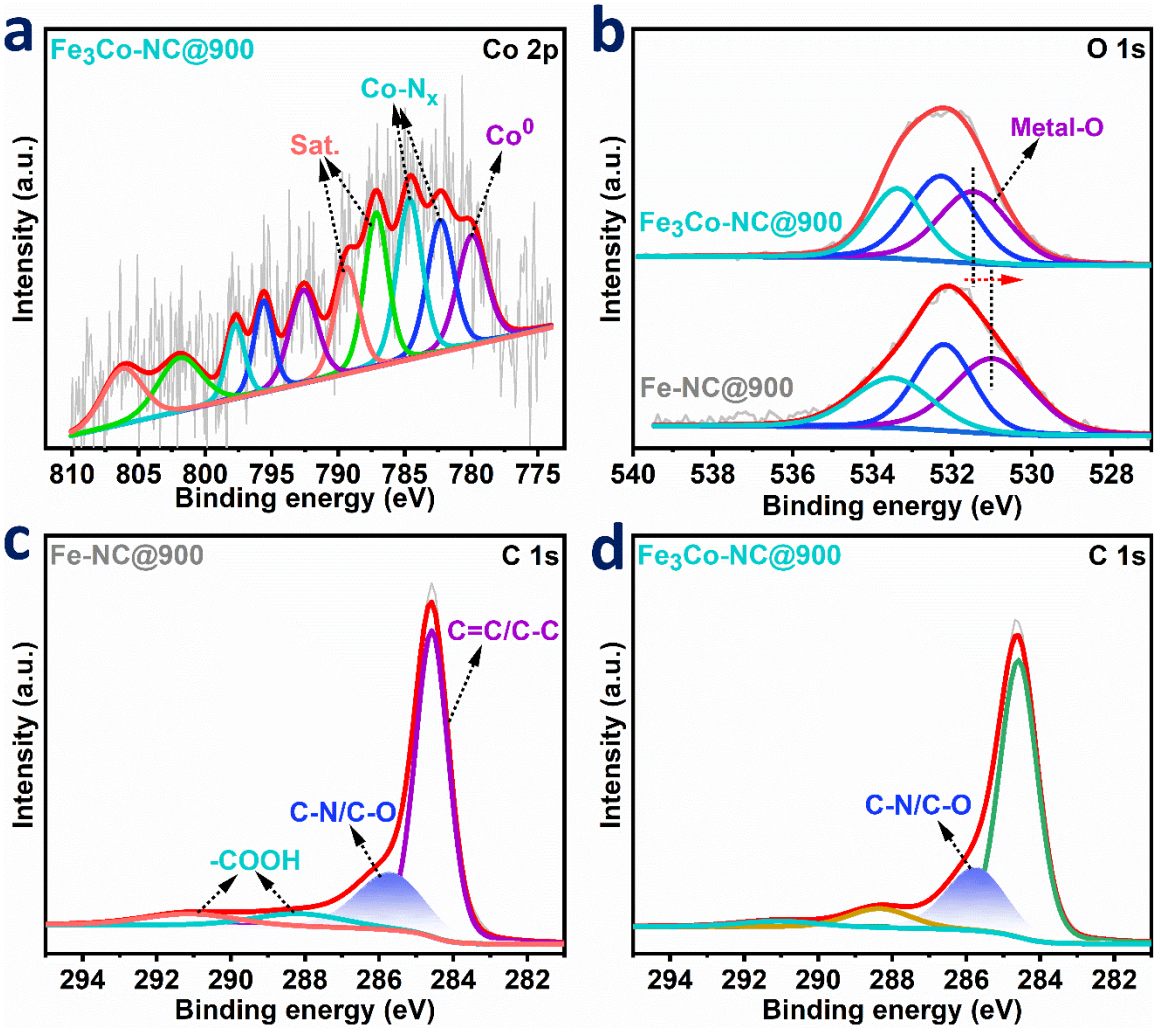

Fig. S4. High-resolution (a) Co 2p XPS spectrum of Fe_3Co-NC@900, and (b) O 1s XPS spectral data of Fe-NC@900 and Fe_3Co-NC@900 and (c,d) C 1s XPS spectral data of Fe-NC@900 and Fe_3Co-NC@900.

	Fe-NC@900	Fe_3Co-NC@900
Pyridinic-N	**31.14**	**30.5**
M-N_x	**18.67**	**19.37**
Pyrrolic-N	**21.37**	**20.66**
Graphitic-N	**14.8**	**20**
Oxidized-N	**14.016**	**9.46**

Table S1. Area percentage of different N species in both Fe-NC@900 and Fe_3Co-NC@900.

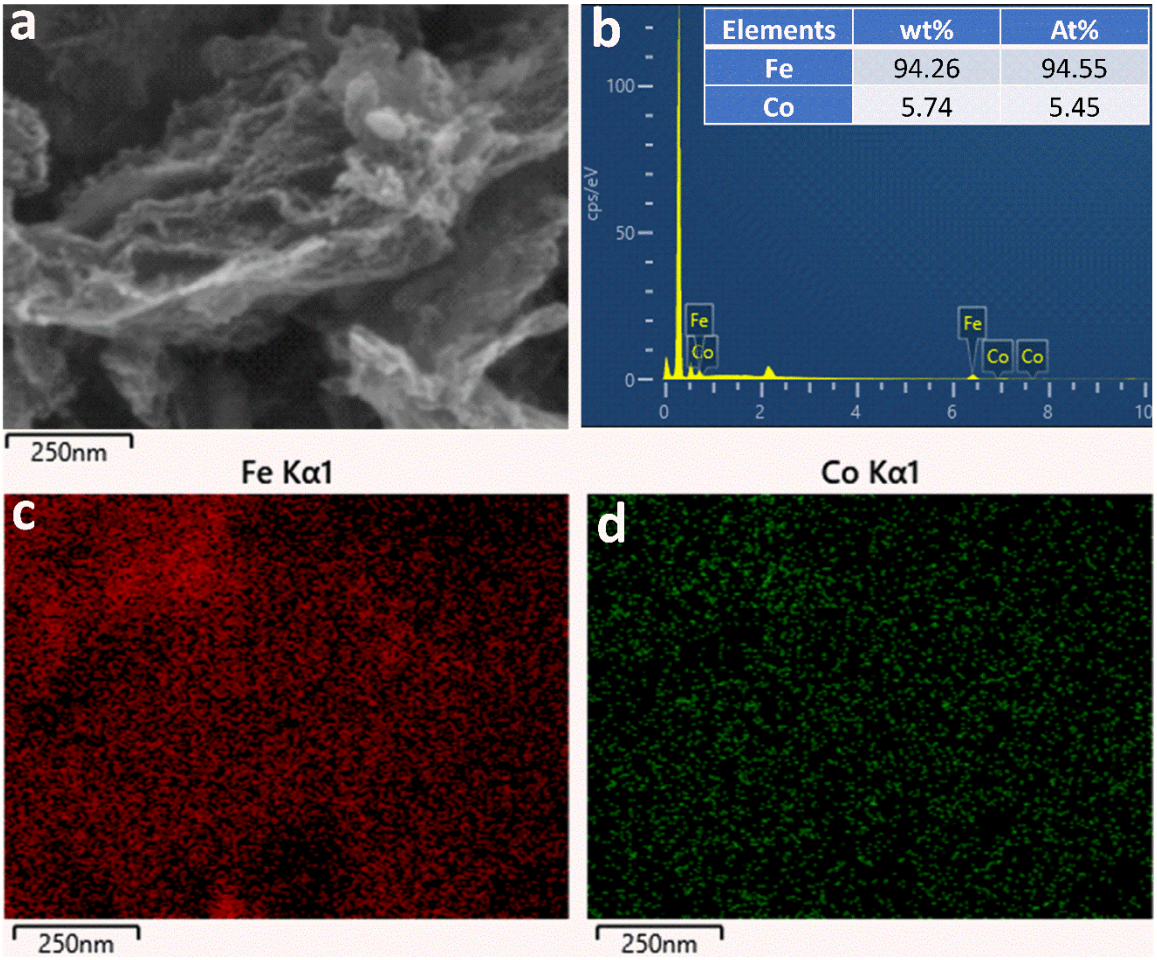

Fig. S5. (a-d) SEM image of Fe_3Co-NC@900 with elemental percentage and the mapping images of Fe and Co elements.

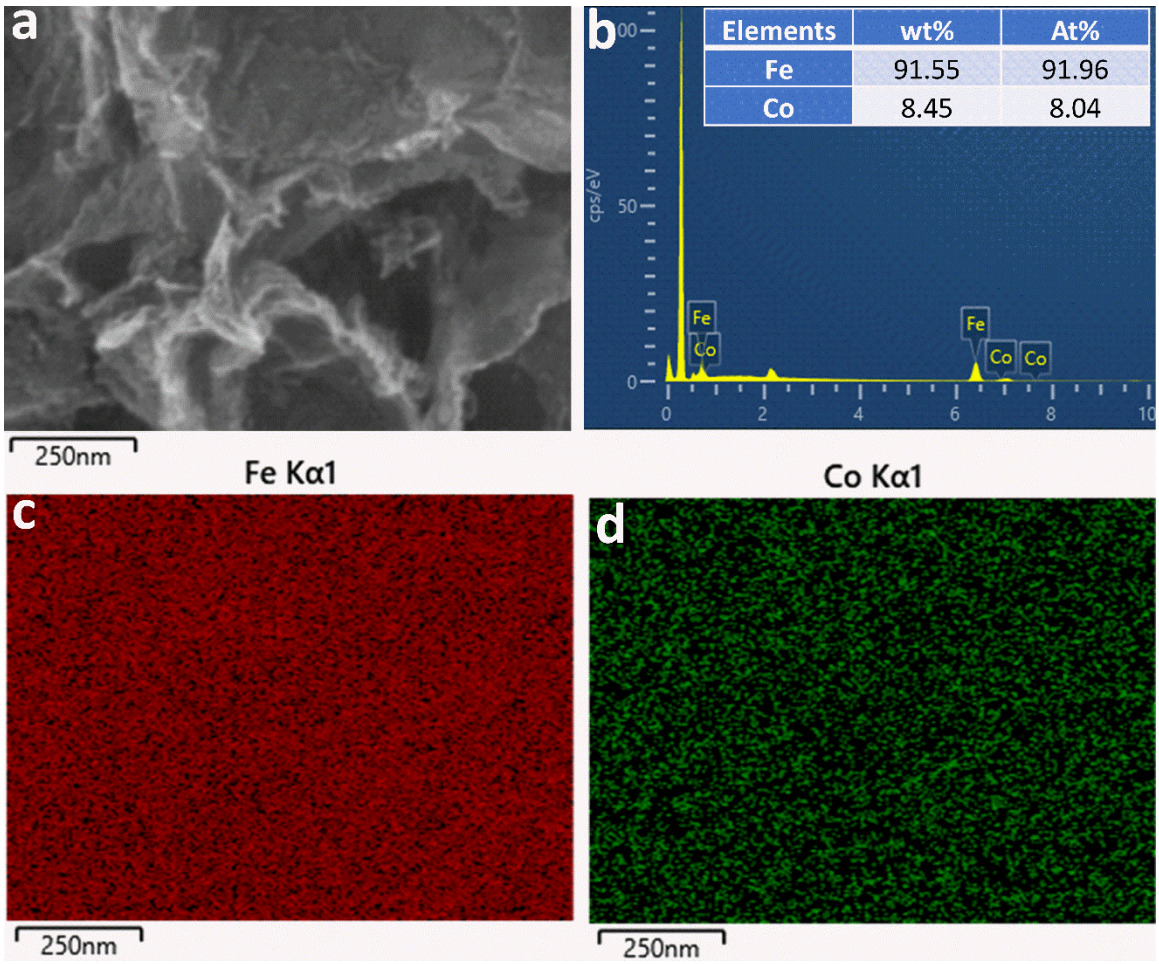

Fig. S6. (a-d) SEM image of FeCo-NC@900 with elemental percentage and the mapping images of Fe and Co elements.

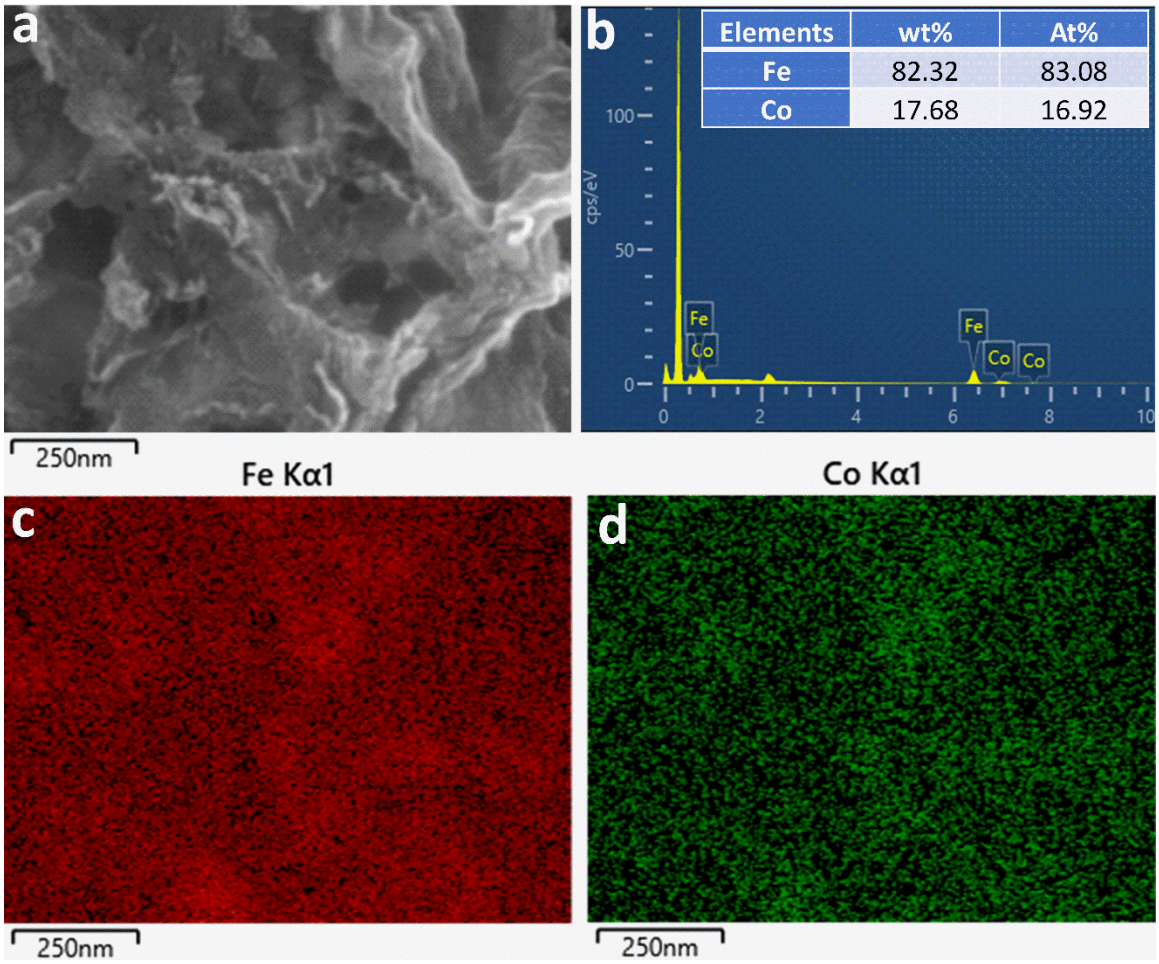

Fig. S7. (a-d) SEM image of $FeCo_3$-NC@900 with elemental percentage and the mapping images of Fe and Co elements.

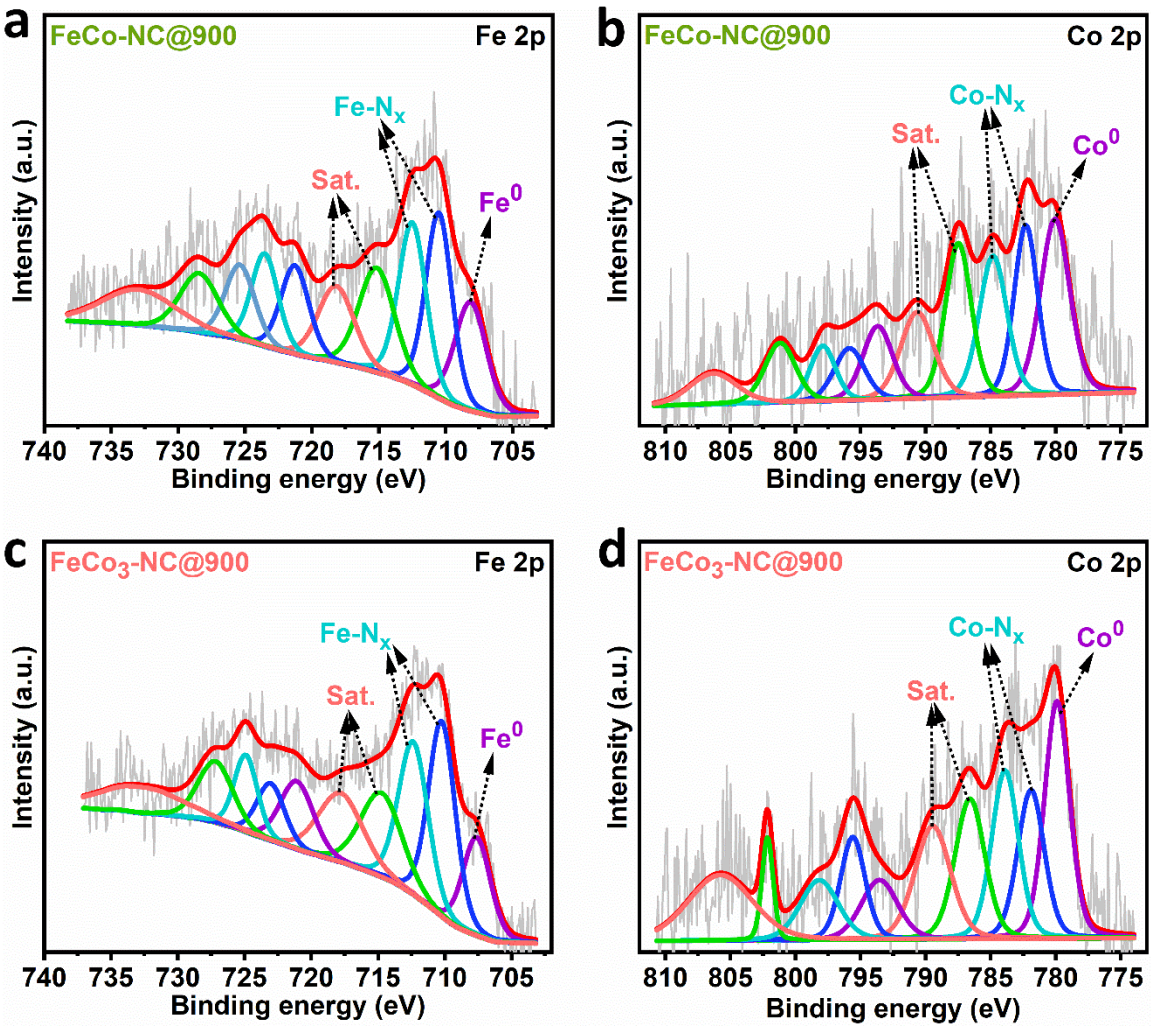

Fig. S8. (a,b) High-resolution Fe 2p and Co 2p XPS spectral data of FeCo-NC@900. (c,d) High-resolution Fe 2p and Co 2p XPS spectral data of $FeCo_3$-NC@900.

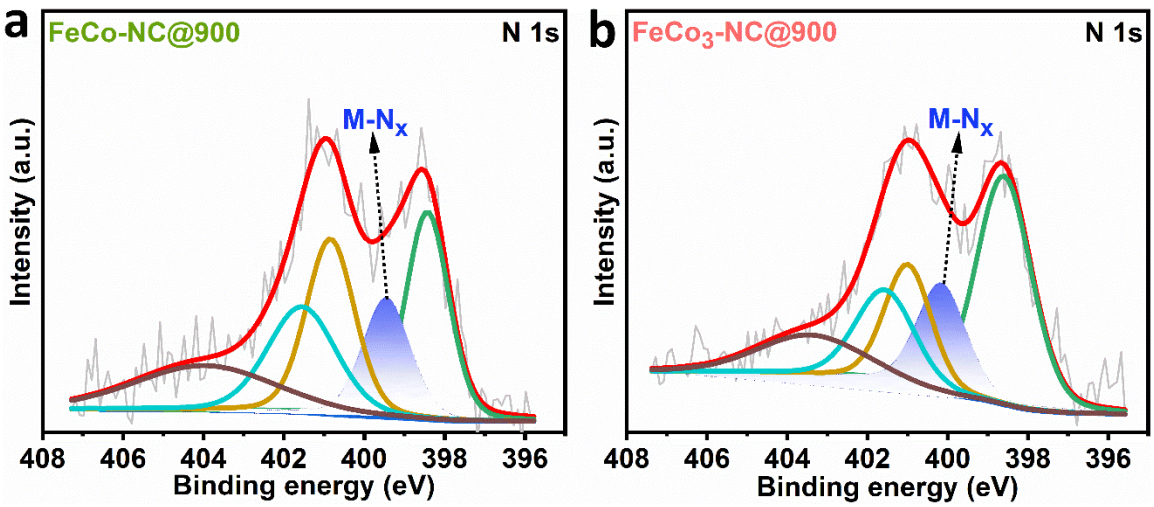

Fig. S9. (a,b) High-resolution N 1s XPS spectral data of FeCo-NC@900, and $FeCo_3$-NC@900, respectively.

	Fe_3Co-NC@900	FeCo-NC@900	$FeCo_3$-NC@900
Pyridinic-N	**30.5**	**24.25**	**37.85**
M-N_x	**19.37**	**15.62**	**16.47**
Pyrrolic-N	**20.66**	**23.2**	**17.1**
Graphitic-N	**20**	**19.78**	**16.16**
Oxidized-N	**9.46**	**17.14**	**12.42**

Table S2. Area percentage of different N species in Fe_3Co-NC@900, Fe-NC@900 and $FeCo_3$-NC@900.

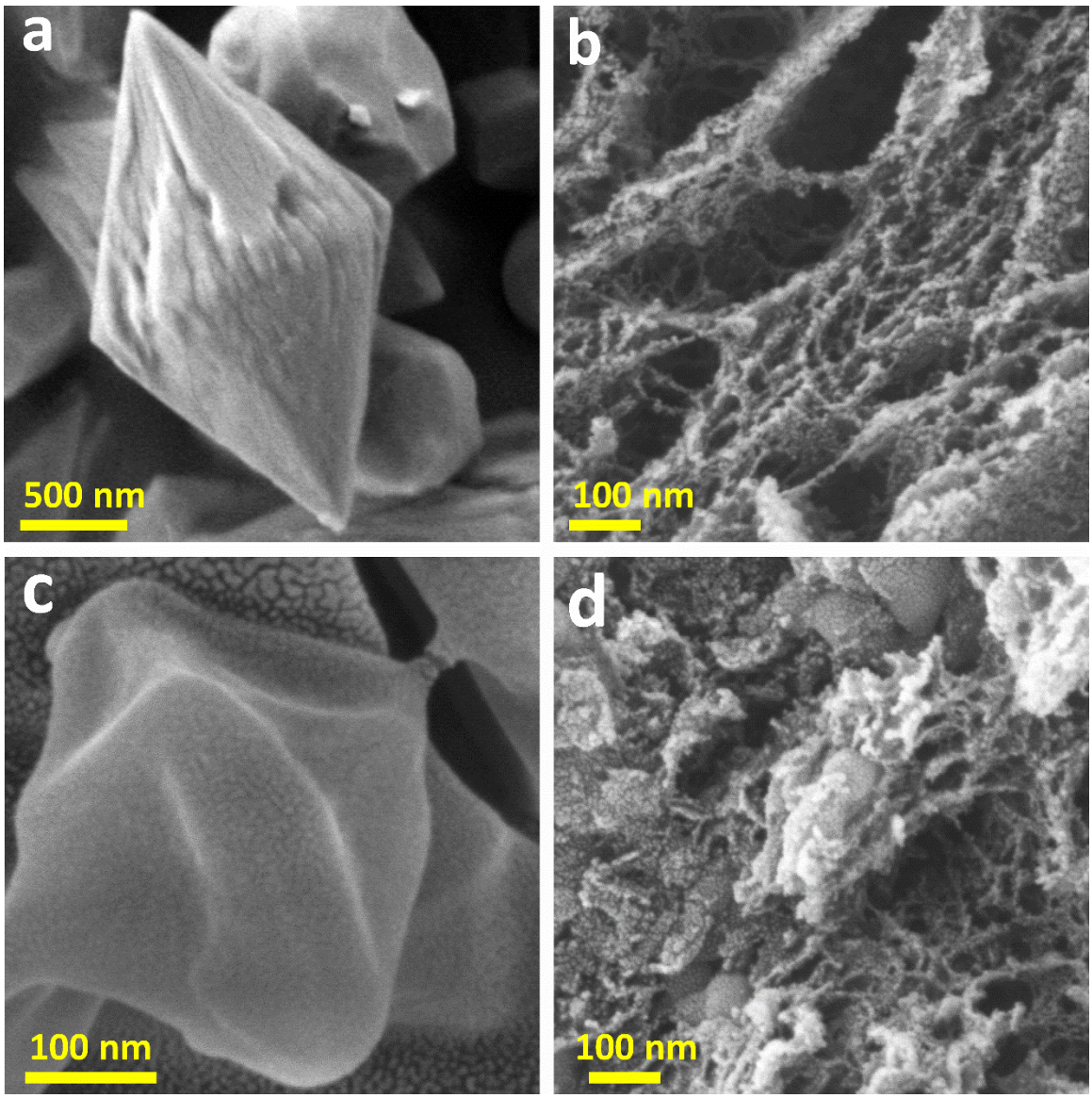

Fig. S10. SEM images of (a) Fe-MIL-53, (b) Fe-NC@900, (c) Fe_3Co-MIL-53, and (d) Fe_3Co-NC@900, respectively.

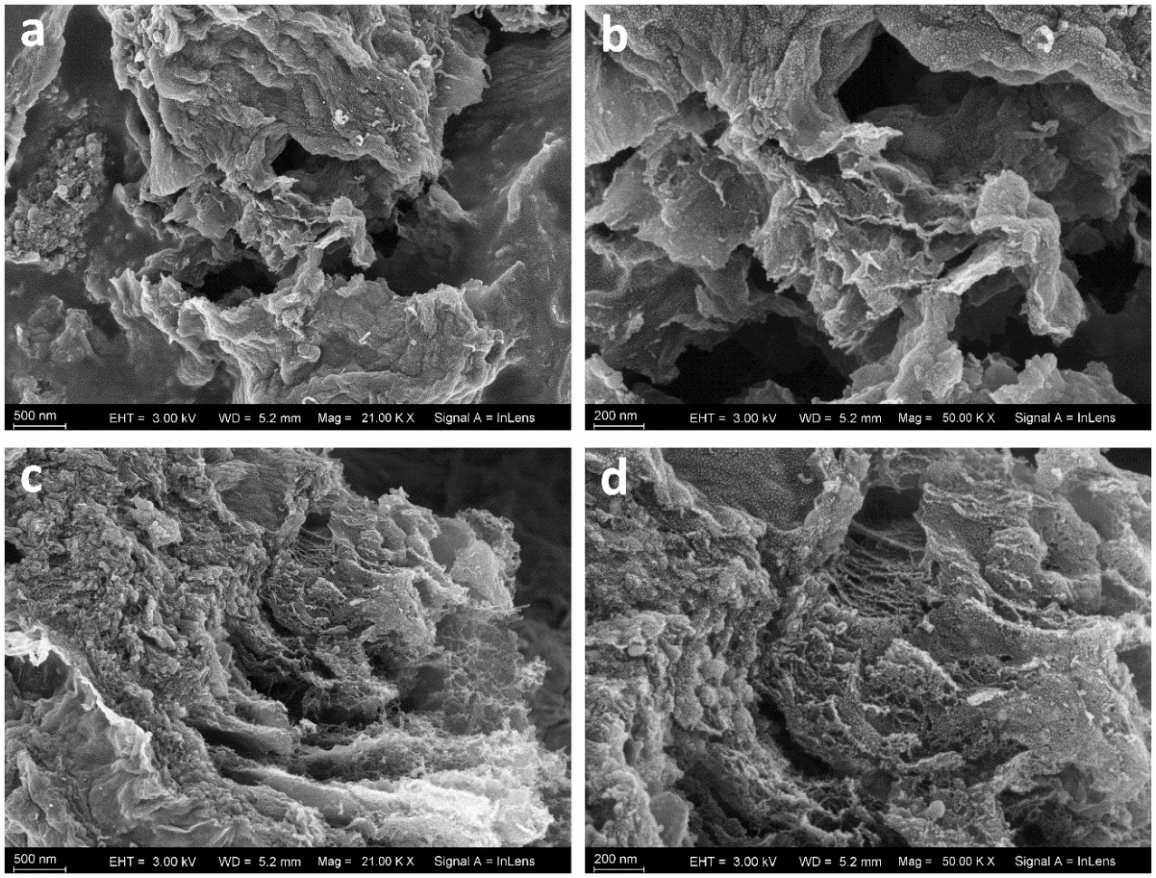

Fig. S11. SEM images of (a,b) FeCo-NC@900, and (c,d) $FeCo_3$-NC@900 at different magnifications.

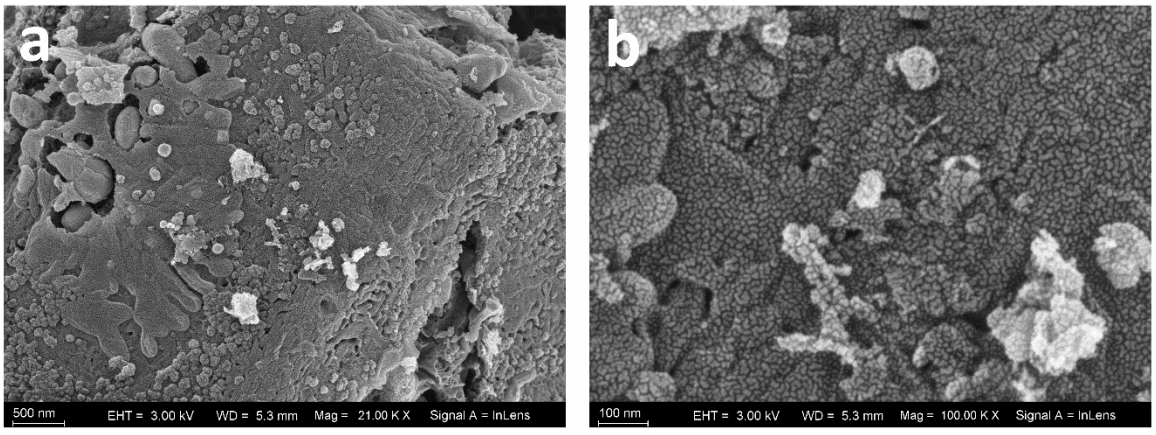

Fig. S12. SEM images of Fe_3Co-C@900 at different magnifications.

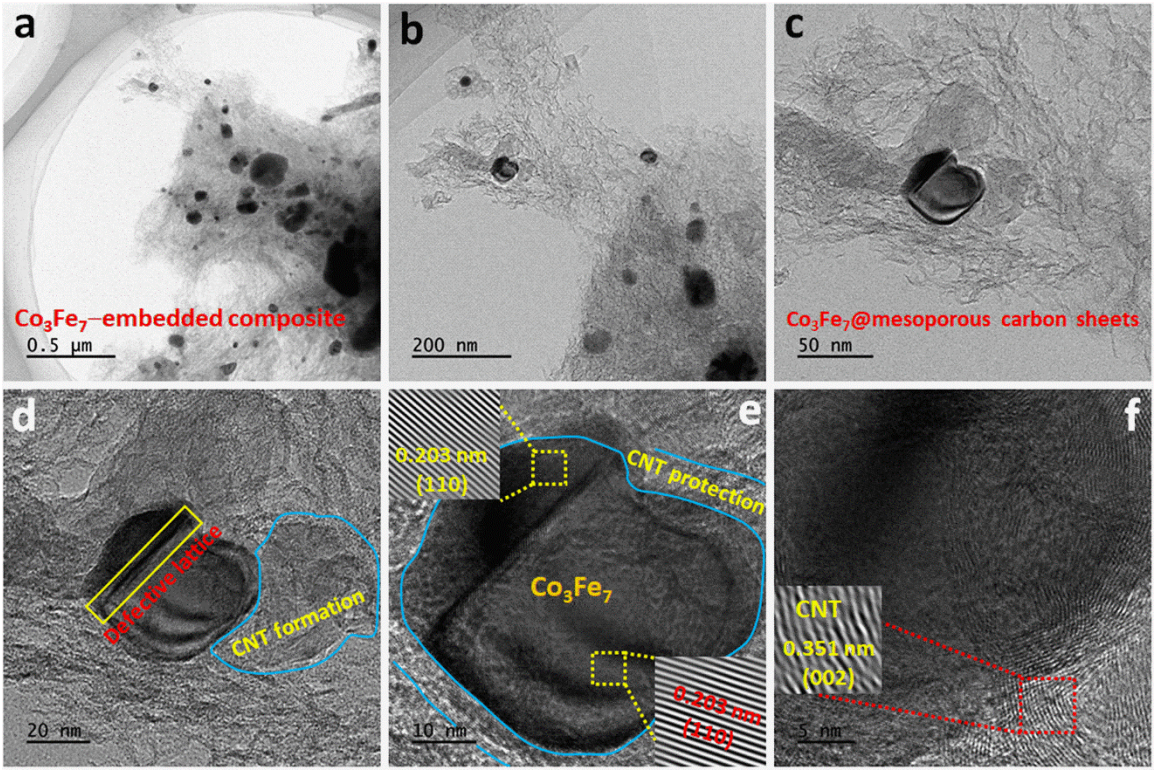

Fig. S13. (a-f) Additional TEM and HR-TEM images of Fe_3Co-NC@900.

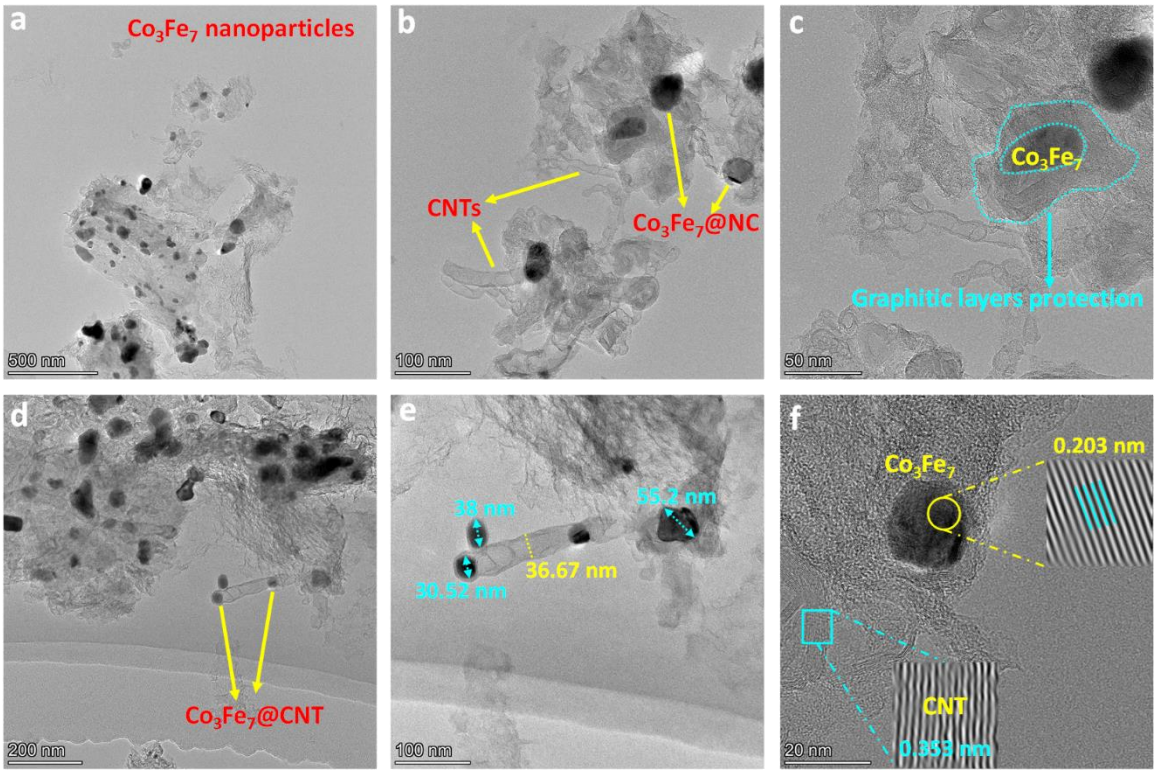

Fig. S14. (a-f) TEM and HR-TEM images of FeCo-NC@900.

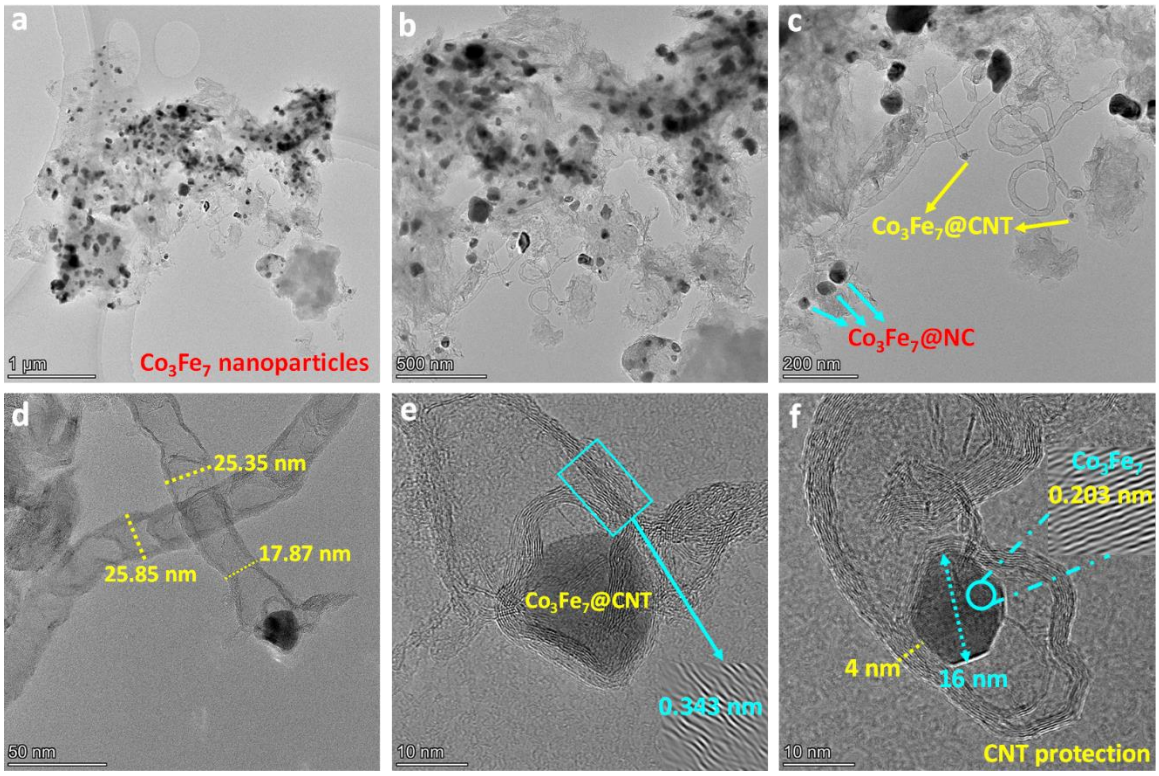

Fig. S15. (a-f) TEM and HR-TEM images of $FeCo_3$-NC@900.

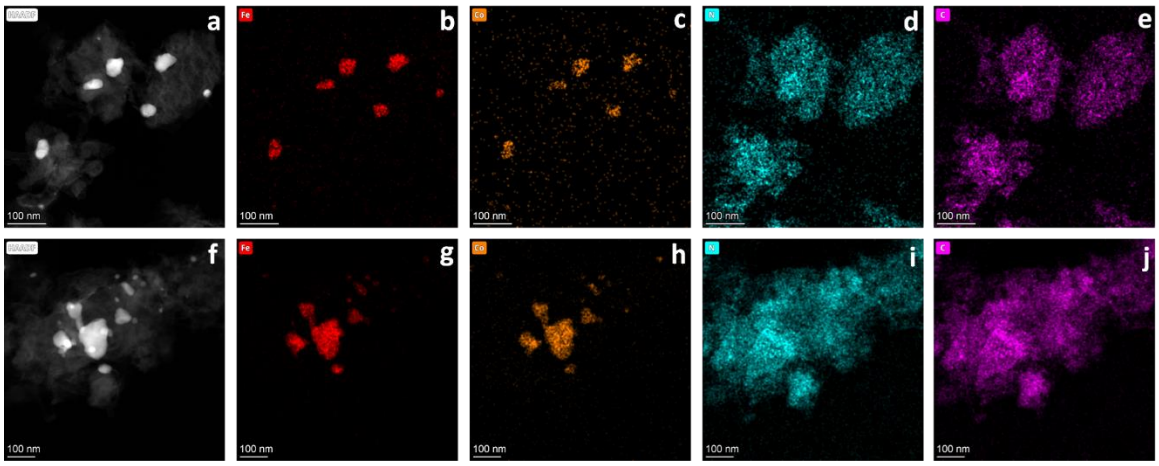

Fig. S16. (a-e) HAADF-STEM and EDS-elemental mapping images of FeCo-NC@900, and (f-j) HAADF-STEM and EDS-elemental mapping images of $FeCo_3$-NC@900.

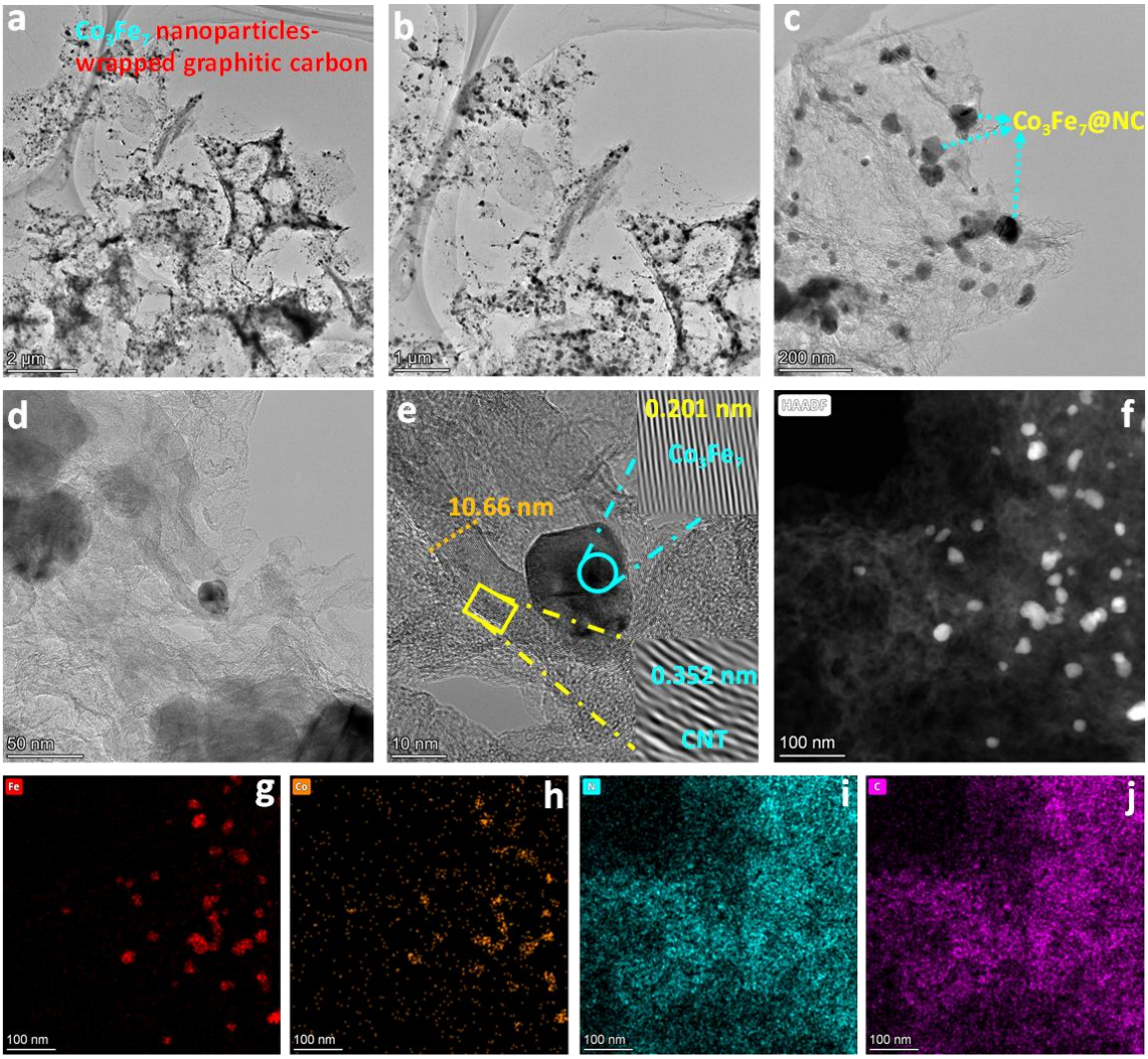

Fig. S17. (a-e) TEM and HR-TEM, (f) HAADF-STEM, and (g-j) the corresponding EDS-mapping images of $Fe_3Co\text{-}NC_5$@900.

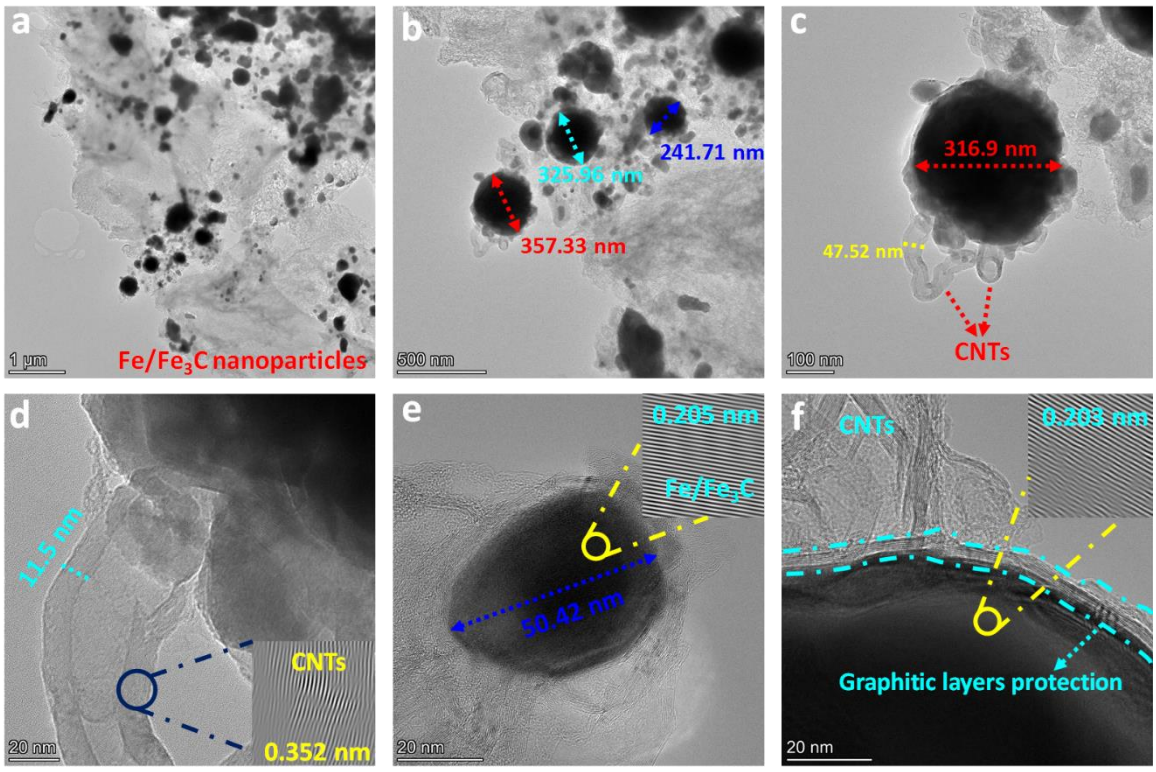

Fig. S18. (a-f) TEM and HR-TEM images of Fe-NC@900.

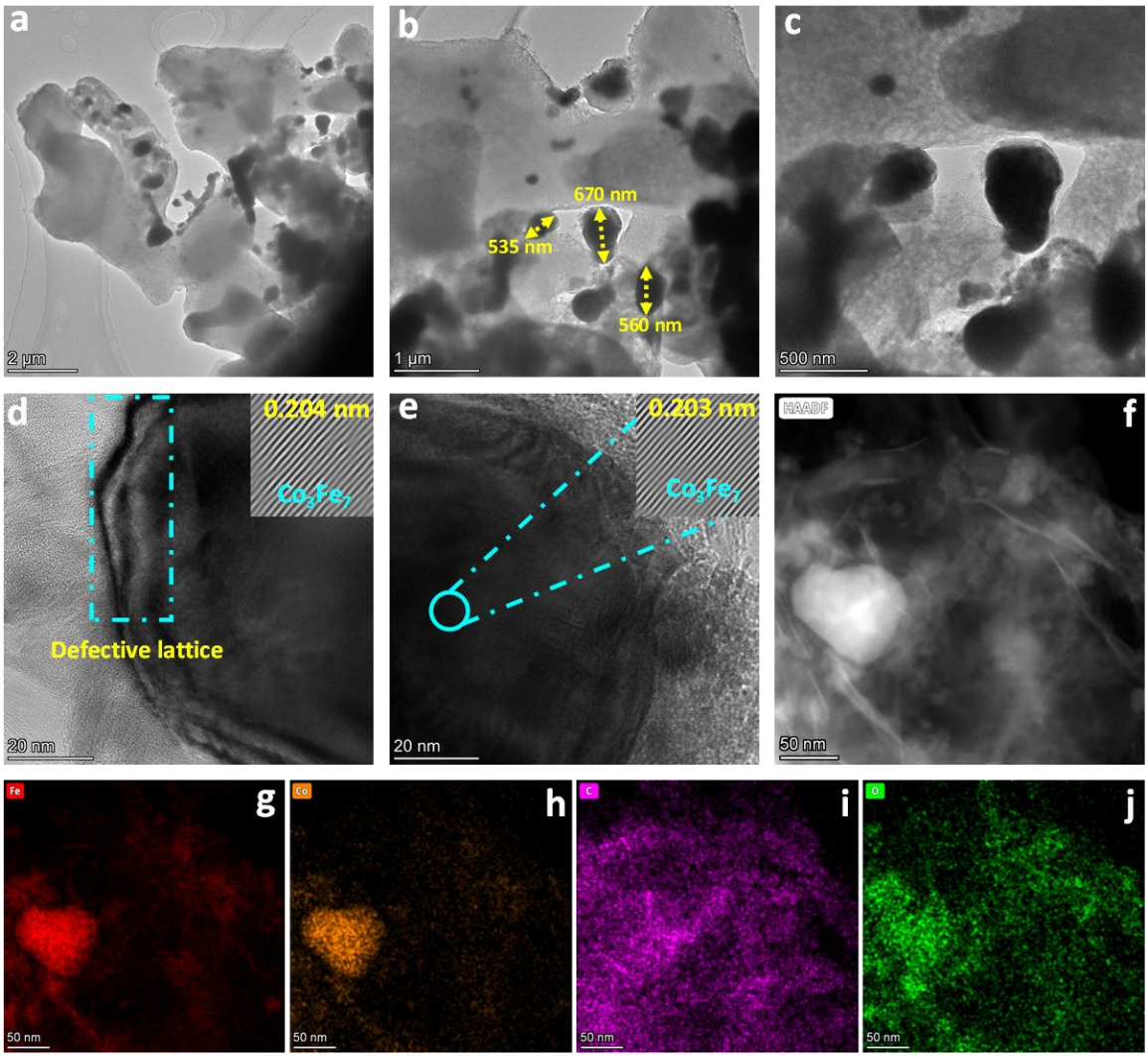

Fig. S19. (a-e) TEM and HR-TEM, (f) HAADF-STEM, and (g-j) the corresponding EDS-mapping images of Fe_3Co-C@900.

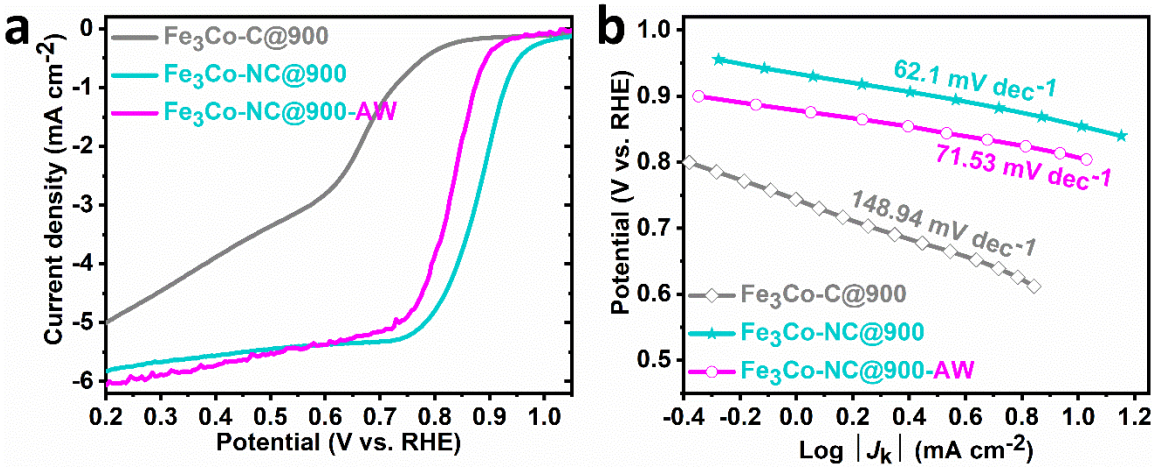

Fig. S20. (a) LSV curves of Fe_3Co-C@900, Fe_3Co-NC@900, and Fe_3Co-NC@900-AW in 0.1 M KOH, (b) corresponding Tafel slopes.

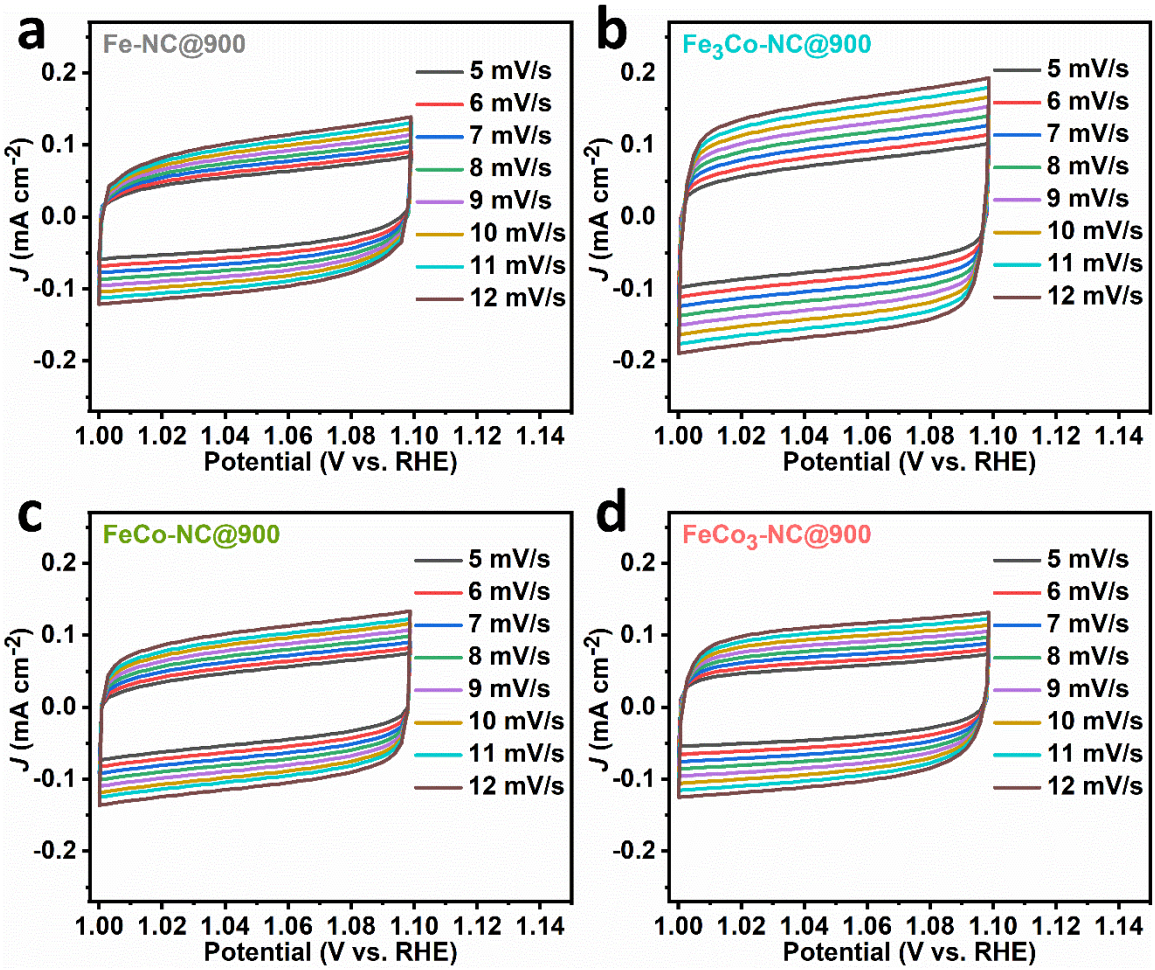

Fig. S21. (a-d) The plots of cyclic voltammograms operated within the non-Faradaic capacitive current range to estimate the ECSA in 0.1 M KOH electrolyte for electrocatalysts, Fe-NC@900, Fe_3Co-NC@900, FeCo-NC@900 and $FeCo_3$-NC@900, respectively.

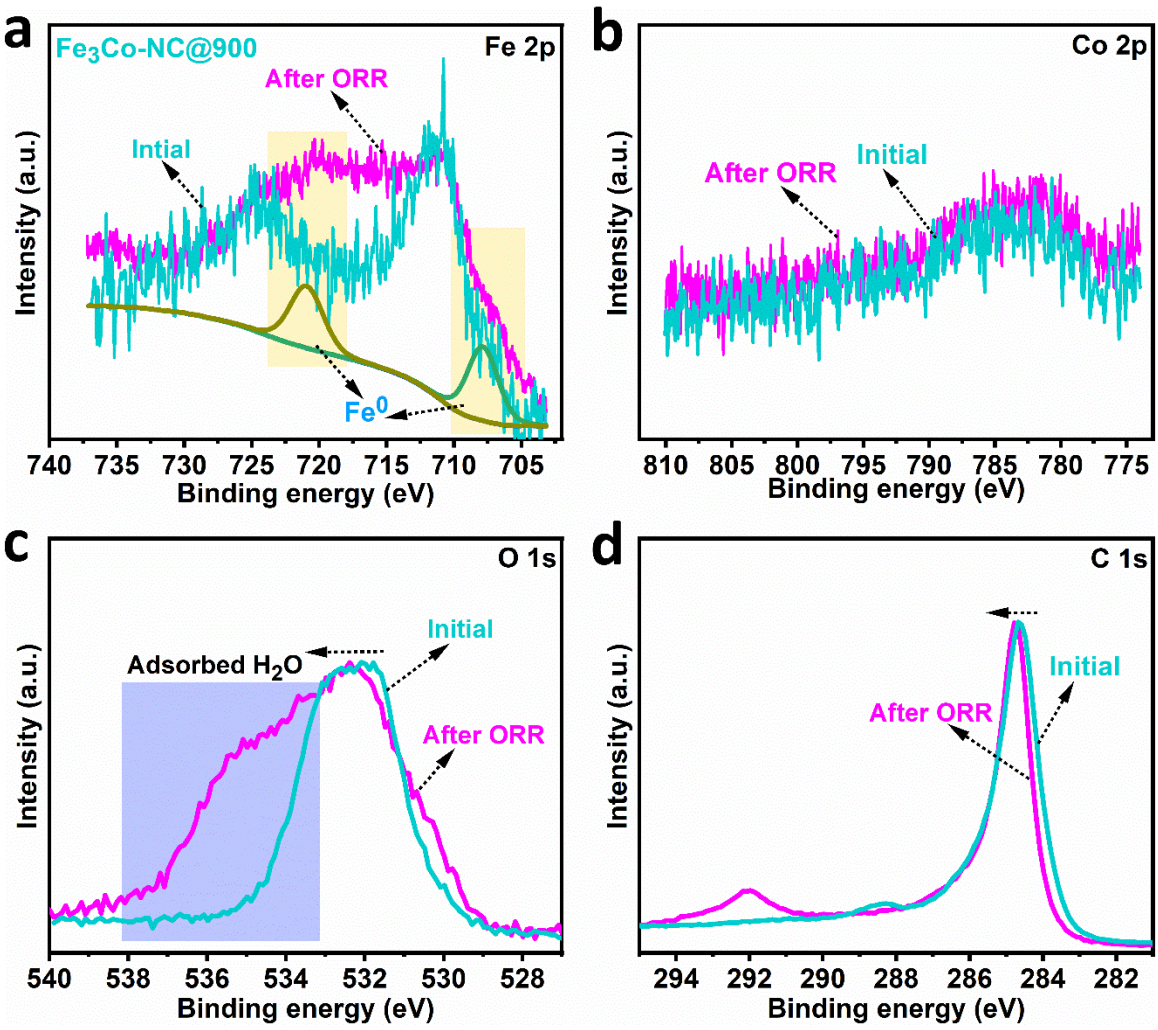

Fig. S22. High-resolution (a) Fe 2p, (b) Co 2p, (c) O 1s and (d) C 1s spectral data of Fe_3Co-NC@900 after ORR.

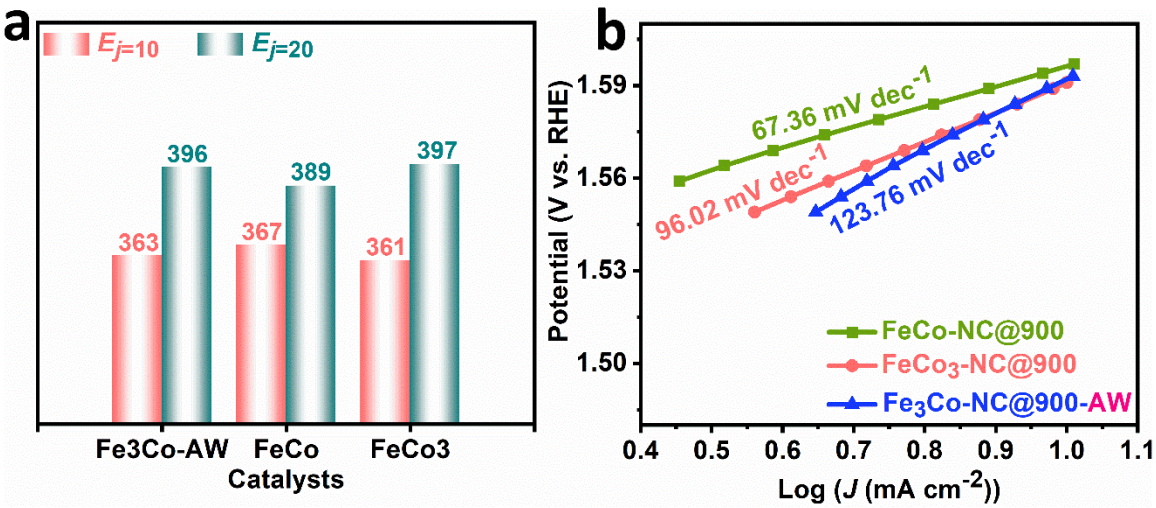

Fig. S23. (a) Overpotential values at 10, and 20 mA cm^{-2} current densities for Fe_3Co-NC@900-AW, FeCo-NC@900, and $FeCo_3$-NC@900 electrocatalysts, (b) Tafel slopes of corresponding electrocatalysts.

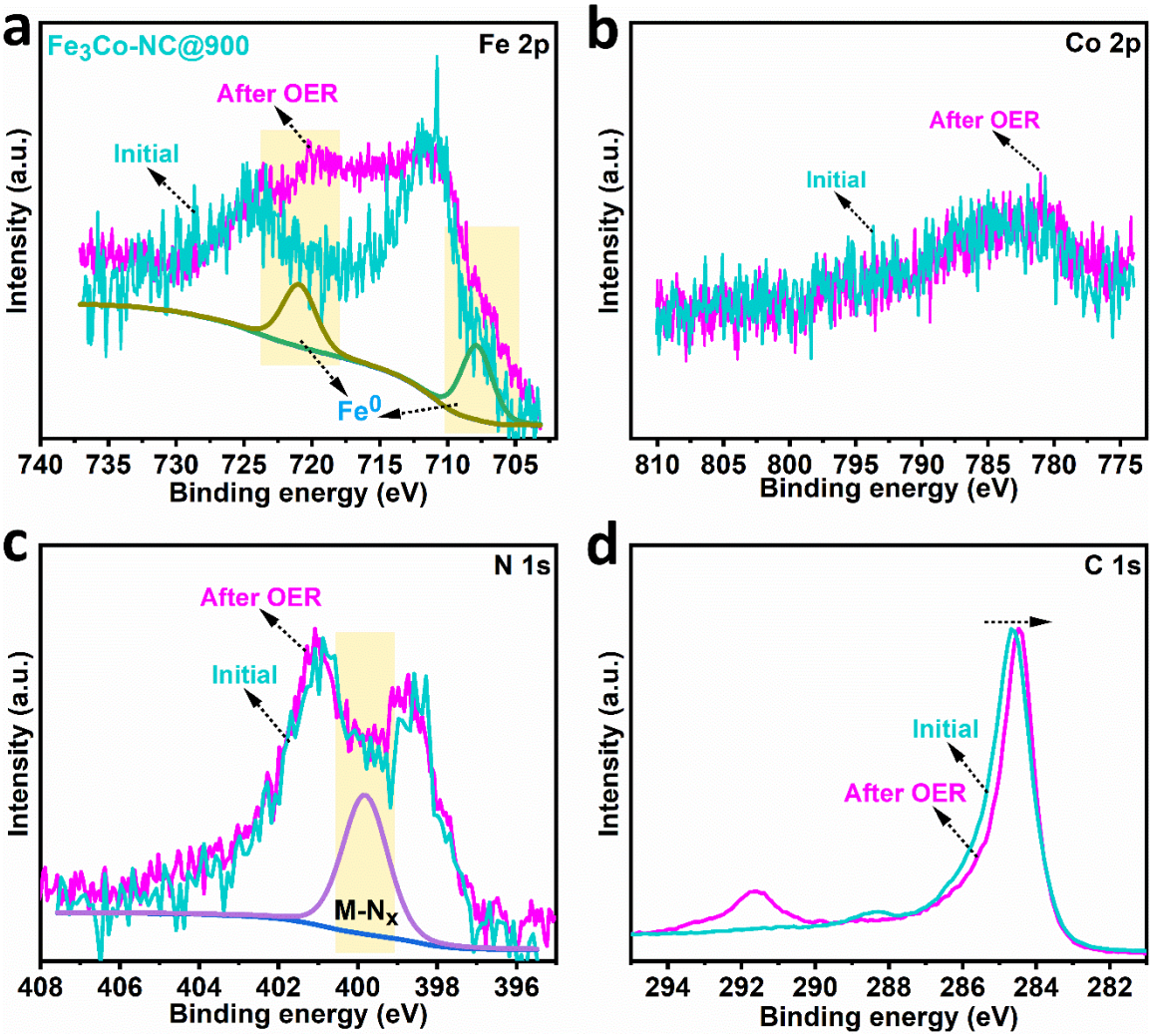

Fig. S24. High-resolution (a) Fe 2p, (b) Co 2p, (c) O 1s and (d) C 1s spectral data of Fe_3Co-NC@900 after ORR.

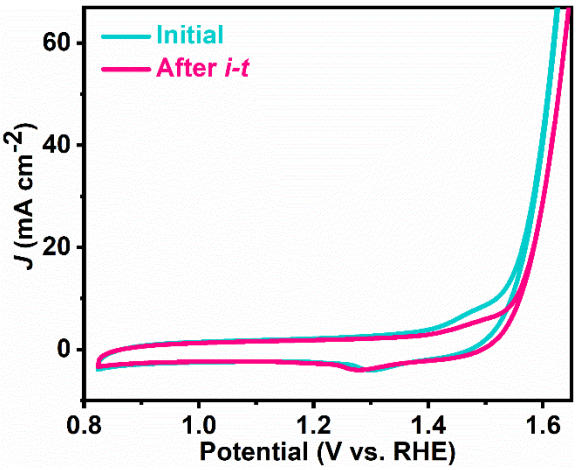

Fig. S25. CV curves obtained before and after the OER *i-t* test on carbon fibre current collector for Fe_3Co-NC@900.

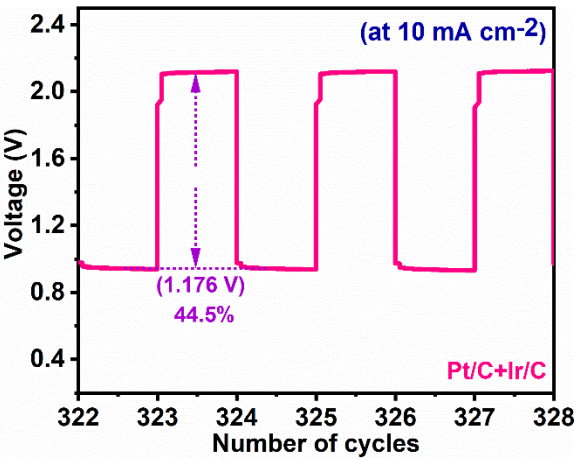

Fig. S26. Zoomed-in view of charge/discharge curves at above 322 cycles for Pt/C+Ir/C-based ZAB.

Table S3: ORR performance of Fe_3Co-NC@900 in comparison with the other **nanoparticles associated SACs or DACs** reported recently in 0.1 M KOH solution.

Materials	E_{onset} (V)	$E_{1/2}$ (V)	J_d at 0.3 V (mA cm^{-2})	Ref.
Fe-NC@900	**0.975**	**0.788**	**5.44**	
Fe_3Co-NC@900	**1.07**	**0.88**	**5.68**	**This work**
Pt/C (20 wt.%)	**1.01**	**0.82**	**5.44**	
Fe,Co/DSA-NSC	NA	0.879	~5.4	[1]
Co_3Fe_7@Co/Fe-SAC	NA	0.841	~5.6	[2]
CoFe/S-NC	NA	0.809	NA	[3]
SA&NP-FeCo-NTS	0.98	0.87	5.7	[4]
Fe/12Zn/Co-NCNTs	1.026	0.879	~5.6	[5]
Co_3Fe_7@$Co_{5.47}$N/NCF	1.02	0.92	~7.0	[6]
FeCo-N,S-G	NA	0.88	~5.2	[7]
FeS/FeNSC	NA	0.91	~5.4	[8]
FeNC	NA	0.88	~5.4	
$FeS/G_{(Fe/GO = 1:4)}$	1.0	0.845	~5.0	[9]
$CoFeS_2$/NC	0.84	0.759	~4.5	[10]
FeS–FeNC@NSC	NA	0.886	5.4	[11]

Fe–S, N–C-950	0.998	0.9	~5.0	[12]
FeS/ZnS@N,S-C-900	1.0	0.88	5.6	[13]
Fe-N-HMCTs	0.992	0.872	5.66	[14]
1MIL/40ZIF-1000	0.97	0.88	4.66	[15]
d-(Co_{NP}/Co_{SA}–N–C)	NA	0.83	≈4.5	[16]
Fe_3C@NCNTs	NA	0.84	5.8	[17]
NP-Fe-NHPC	0.97	0.88	≈5.1	[18]
SA-Fe-NHPC	1.01	0.93	≈6.0	[18]
PA@Z8-Fe-N-C Z8-Fe-N-C	NA NA	0.88 0.83	≈5.2 ≈5.0	[19]
FeSA-FeNC@NSC	NA	0.90	≈5.0	[20]
Fe_3C–FeN/NC	0.95	0.80	5.1	[21]
Fe_3C@NPW	NA	0.87	≈5.2	[22]
Fe_3C@N/MCHSs	1.01	0.875	≈5.4	[23]

Abbreviations: NA = not available; DSA-NSC = dual single atoms-embedded N/S-doped Carbon; SA&NP-FeCo-NTS = bimetallic atomic FeN_4, CoN_4, and FeCo alloy nanoparticles and a unique nanotube-assembled-sphere; NCNTs = N-doped carbon nanotubes; NCF = nitrogen-doped carbon foam; FeCo-N,S-G = Fe, Co, N, and S co-doped three-dimensional (3D) porous graphene-like catalyst; FeS/FeNSC represents Fe-N_4 sites

and FeS nanoparticles embedded N/S-doped carbon; FeS/G = iron sulfide/graphene oxide; NC = N-doped carbon and NSC = N/S-co-doped carbon; N-HMCTs = N-doped hollow mesoporous carbon tubes, consists of Fe-N_x and Fe_3C; 1MIL/40ZIF-1000 consists of Fe-N-C sites and Fe-Fe_3C; d-(Co_{NP}/Co_{SA}–N–C) consists of CoN_4 sites and Co; In Fe_3C@NCNTs, NCNTs = N-doped carbon nanotubes, consists of Fe-N_4 sites and Fe_3C; In NP-Fe-NHPC, NHPC = hierarchically porous carbon, consists of single atom Fe-N_x sites and Fe nanoparticles; In SA-Fe-NHPC, SA = Fe single atom sites; In PA@Z8-Fe-N-C; PA = phenylboronic acid, Z8 = ZIF-8, N-C = N-doped carbon, consists of Fe-N-C sites; Z8-Fe-N-C consists of Fe-N-C sites and Fe nanoparticles; In FeSA-FeNC@NSC, SA = single atom, NC= Nanocluster, NSC = N/S co-doped porous carbon, consists of Fe-N-C sites and Fe-nanoclusters; Fe_3C–FeN/NC consists of Fe_3C nanoparticles and Fe-N_4 sites; In Fe_3C@NPW, NPW = paulownia wood-derived N-doped carbon, consists of Fe_3C nanoparticles; In Fe_3C@N/MCHSs, MCHSs = mesoporous carbon hollow spheres, consists of Fe_3C nanoparticles.

Table S4: Bifunctional activity of Fe_3Co-NC@900 in comparison with state-of-the-art electrocatalysts that have better or comparable bifunctional activity parameter (**Δ*E***).

Materials	$E_{1/2}$ **(V)**	$E_{j=10}$ **(V)**	**ΔE (V)**	**Ref.**
Fe-NC@900	**0.788**	**1.608**	**0.82**	
Fe_3Co-NC@900	**0.88**	**1.572**	**0.692**	**This work**
Pt/C (ORR) + Ir/C (OER)	**0.82**	**1.568**	**0.748**	
Fe,Co/DSA-NSC	0.879	1.44	**0.561**	[1]
PCL113	0.918	1.498	**0.580**	[24]
ls-PCL	0.923	1.514	**0.591**	
FeCo-NPCNs	0.87	1.47	**0.60**	[25]
AlNiCoRuMoCrFeTi	0.865	1.47	**0.61**	[26]
FeCo@MNC	0.86	1.47	**0.62**	[27]
CoNC@LDH	0.84	1.47	**0.63**	[28]
Fe-Phen-800	0.878	1.515	**0.637**	[29]
MnO_2-NiFe	0.80	1.45	**0.65**	[30]
MnSAC	0.915	1.58	**0.665**	[31]
S-$Co_{9-x}Fe_xS_8$@rGO	0.84	1.51	**0.67**	[32]
FAS-NSC@950	0.871	1.544	**0.673**	[33]

NiS_x/NMC	0.89	1.57	**0.68**	[34]
CoFe-LDH@FeCo NPs-N-CNTs	0.87	1.55	**0.68**	[35]
Fe_3C|Fe-N-C	0.888	1.568	**0.68**	[36]
FeS/Fe_3C@NS-C-900	0.78	1.5	**0.72**	[37]
CoFe/S-N-C	0.844	1.588	**0.744**	[3]
Fe, Co/N-C	0.86	1.618	**0.75**	[38]
SAC-FeN-WPC	0.85	1.63	**0.78**	[39]
Fe_3C@NG800-0.2	0.811	1.591	**0.78**	[40]
FeCo-1/NSC	0.82	1.555	**0.83**	[41]
FeCo-NCNFs-800	0.817	1.686	**0.869**	[42]

Abbreviations: PCL113 = is a special terminology for NiFeLDH+COP_{BTC}+CNTs; ls-PCL = Carbon black supported PCL113; AlNiCoRuMoCrFeTi = Eight-component high-entropy oxide; LDHs = layered double hydroxides; Phen = 1,10-phenanthroline monohydrate; SAC = single-atom catalyst; rGO = reduced Graphene Oxide; NMC = nitrogen-doped mesoporous carbon; CoFe-LDH@FeCo NPs-N-CNTs = CoFe-layer double hydroxide@FeCo nanoparticles embedded in N-doped carbon nanotubes; NS-C = N,S-dual doped carbon; WPC = wood-based porous carbon; and NG = N-doped graphitic layers.

References:

1 G. Yasin, S. Ali, S. Ibraheem, A. Kumar, M. Tabish, M. A. Mushtaq, S. Ajmal, M. Arif, M. A. Khan, A. Saad, L. Qiao and W. Zhao, *ACS Catal.*, 2023, **13**, 2313–2325.

2 B. Liu, S. Wang, R. Feng, Y. Ni, F. Song and Q. Liu, *ACS Appl. Mater. Interfaces*, 2022, **14**, 38739–38749.

3 G. Li, Y. Tang, T. Fu, Y. Xiang, Z. Xiong, Y. Si, C. Guo and Z. Jiang, *Chem. Eng. J.*, 2022, **429**, 132174.

4 Q. Zhang, P. Liu, X. Fu, Y. Yuan, L. Wang, R. Gao, L. Zheng, L. Yang and Z. Bai, *Adv. Funct. Mater.*, 2022, **32**, 2112805.

5 J. Xue, S. Deng, R. Wang and Y. Li, *Carbon N. Y.*, 2023, **205**, 422–434.

6 M. Jiang, C. Fu, R. Cheng, W. Zhang, T. Liu, R. Wang, J. Zhang and B. Sun, *Adv. Sci.*, 2020, **7**, 2000747.

7 Y. Liu, W. Duan, H. Pei, P. Sun, Y. Sun, Y. Zhuang and Z. Li, *ACS Appl. Energy Mater.*, 2023, **6**, 7194–7204.

8 J. Chen, B. Huang, R. Cao, L. Li, X. Tang, B. Wu, Y. Wu, T. Hu, K. Yuan and Y. Chen, *Adv. Funct. Mater.*, 2023, **33**, 2209315.

9 J. Gautam, D. T. Tran, T. I. Singh, N. H. Kim and J. H. Lee, *J. Power Sources*, 2019, **427**, 91–100.

10 J. Cai, H. Liu, Y. Luo, Y. Xiong, L. Zhang, S. Wang, K. Xiao and Z.-Q. Liu, *J. Energy Chem.*, 2022, **74**, 420–428.

11 Z. Chen, R. Liu, S. Liu, J. Huang, L. Chen, R. Nadimicherla, D. Wu and R. Fu, *Chem. Commun.*, 2020, **56**, 12921–12924.

12 H. Xu, D. Wang, P. Yang, A. Liu, R. Li, L. Xiao, J. Zhang, Z. Qu and M. An, *Sustain. Energy Fuels*, 2021, **5**, 2695–2703.

13 R. Jiang, X. Chen, J. Deng, T. Wang, K. Wang, Y. Chen and J. Jiang, *J. Energy Chem.*, 2020, **47**, 79–85.

14 X. Cui, L. Gao, S. Lei, S. Liang, J. Zhang, C. D. Sewell, W. Xue, Q. Liu, Z. Lin and Y. Yang, *Adv. Funct. Mater.*, 2021, **31**, 2009197.

15 H. Wang, F. Yin, N. Liu, R. Kou, X. He, C. Sun, B. Chen, D. Liu and H. Yin, *Adv. Funct. Mater.*, 2019, **29**, 1901531.

16 X. Cheng, J. Yang, W. Yan, Y. Han, X. Qu, S. Yin, C. Chen, R. Ji, Y. Li, G. Li, G. Li, Y. Jiang and S. Sun, *Energy Environ. Sci.*, 2021, **14**, 5958–5967.

17 C. Xu, C. Guo, J. Liu, B. Hu, J. Dai, M. Wang, R. Jin, Z. Luo, H. Li and C. Chen, *Energy Storage Mater.*, 2022, **51**, 149–158.

18 G. Chen, P. Liu, Z. Liao, F. Sun, Y. He, H. Zhong, T. Zhang, E. Zschech, M. Chen, G. Wu, J. Zhang and X. Feng, *Adv. Mater.*, 2020, **32**, 1907399.

19 L. Gao, X. Gao, P. Jiang, C. Zhang, H. Guo and Y. Cheng, *Small*, 2022, **18**,

2105892.

20 W. Zhai, S. Huang, C. Lu, X. Tang, L. Li, B. Huang, T. Hu, K. Yuan, X. Zhuang and Y. Chen, *Small*, 2022, **18**, 2107225.

21 F. Zhou, P. Yu‡, F. Sun, G. Zhang, X. Liu and L. Wang, *J. Mater. Chem. A*, 2021, **9**, 6831–6840.

22 M. Cao, Y. Liu, K. Sun, H. Li, X. Lin, P. Zhang, L. Zhou, A. Wang, S. Mehdi, X. Wu, J. Jiang and B. Li, *Small*, 2022, **18**, 2202014.

23 X. Yang, X. Zheng, H. Li, B. Luo, Y. He, Y. Yao, H. Zhou, Z. Yan, Y. Kuang and Z. Huang, *Adv. Funct. Mater.*, 2022, **32**, 2200397.

24 X. Li, D. Liu, Q. Liu and Z. Xiang, *Small*, 2022, **18**, 2201197.

25 L. Lin, P. Xue, X. Cui, J. Liu, J. Liu, M. Tang and Z. Wang, *J. Alloys Compd.*, 2022, **909**, 164625.

26 Z. Jin, J. Lyu, K. Hu, Z. Chen, G. Xie, X. Liu, X. Lin and H. Qiu, *Small*, 2022, **18**, 2107207.

27 C. Li, M. Wu and R. Liu, *Appl. Catal. B Environ.*, 2019, **244**, 150–158.

28 C. Zhao, J. Liu, J. Wang, D. Ren, J. Yu, X. Chen, B. Li and Q. Zhang, *Adv. Mater.*, 2021, **33**, 2008606.

29 K. Srinivas, Z. Chen, F. Ma, A. Chen, Z. Zhang, Y. Wu, M. Zhu and Y. Chen, *Appl. Catal. B Environ.*, 2023, **335**, 122887.

30 P. Wang, Y. Lin, L. Wan and B. Wang, *ACS Appl. Mater. Interfaces*, 2019, **11**, 37701–37707.

31 H. Shang, W. Sun, R. Sui, J. Pei, L. Zheng, J. Dong, Z. Jiang, D. Zhou, Z. Zhuang, W. Chen, J. Zhang, D. Wang and Y. Li, *Nano Lett.*, 2020, **20**, 5443–5450.

32 T. Liu, F. Yang, G. Cheng and W. Luo, *Small*, 2018, **14**, 1703748.

33 K. Srinivas, Z. Chen, A. Chen, F. Ma, M. Zhu and Y. Chen, *J. Energy Chem.*, 2024, **90**, 565–577.

34 K. Wan, J. Luo, X. Zhang, C. Zhou, J. W. Seo, P. Subramanian, J. Yan and J. Fransaer, *J. Mater. Chem. A*, 2019, **7**, 19889–19897.

35 T. Zhang, J. Bian, Y. Zhu and C. Sun, *Small*, 2021, **17**, 2103737.

36 Y. Chen, X. Kong, Y. Wang, H. Ye, J. Gao, Y. Qiu, S. Wang, W. Zhao, Y. Wang, J. Zhou and Q. Yuan, *Chem. Eng. J.*, 2023, **454**, 140512.

37 Y. W. Li, W. J. Zhang, J. Li, H. Y. Ma, H. M. Du, D. C. Li, S. N. Wang, J. S. Zhao, J. M. Dou and L. Xu, *ACS Appl. Mater. Interfaces*, 2020, **12**, 44710–44719.

38 W. Yang, J. Guo, J. Ma, N. Wu, J. Xiao and M. Wu, *J. Alloys Compd.*, 2022, **926**, 166937.

39 L. Zhong, C. Jiang, M. Zheng, X. Peng, T. Liu, S. Xi, X. Chi, Q. Zhang, L. Gu, S. Zhang, G. Shi, L. Zhang, K. Wu, Z. Chen, T. Li, M. Dahbi, J. Alami, K. Amine and J. Lu, *ACS Energy Lett.*, 2021, **6**, 3624–3633.

40 H. Jiang, Y. Yao, Y. Zhu, Y. Liu, Y. Su, X. Yang and C. Li, *ACS Appl. Mater. Interfaces*, 2015, **7**, 21511–21520.

41 S. Chang, H. Zhang and Z. Zhang, *J. Energy Chem.*, 2021, **56**, 64–71.

42 L. Yang, S. Feng, G. Xu, B. Wei and L. Zhang, *ACS Sustain. Chem. Eng.*, 2019, **7**, 5462–5475.